Adiabatic coherent control in the anharmonic ion trap: Proposal for the vibrational two-qubit system

Lei Wang and Dmitri Babikov*
Chemistry Department, Marquette University, P.O. Box 1881, Milwaukee, Wisconsin 53201, USA
(Received 13 January 2011; published 20 May 2011)

A method for encoding a multiqubit system into the quantized motional states of ion string in an anharmonic linear trap is proposed. Control over this system is achieved by applying oscillatory electric fields (rf) shaped optimally for desired state-to-state transitions. Anharmonicity of the vibrational spectrum of the system plays a key role in this approach to the control and quantum computation, since it allows resolving different state-to-state transitions and addressing them selectively. The anharmonic trap architecture proposed earlier [Phys. Rev. A **83**, 022305 (2011)] is explored here and the optimal control theory is used to derive pulses for a set of universal quantum gates. An accurate choice of pulse parameters allows deriving gates that are both accurate and simple. A practical realization of this approach seems to be within the reach of today's technology.

DOI: 10.1103/PhysRevA.83.052319 PACS number(s): 03.67.Lx, 37.10.Ty

I. INTRODUCTION

A string of atomic ions trapped and cooled in a linear Paul trap represents a man-made quantum system well isolated from the environment. Favorable properties of this system, such as a long coherence time and the possibility of fast and reliable manipulations with its quantum states, make it suitable for the practical realization of quantum computation. In the original proposal of Cirac and Zoller [1], qubits are encoded into electronic states of ions and quantum gates are achieved by laser excitation of ions, dependent on their motional eigenstate. The motional mode of multiple ions in the trapping potential is used to create entanglement. Realization of this proposal in the experiment [2] led to many fascinating developments and the explosive growth of the field [3–17].

While the architecture of Cirac and Zoller relies mostly on the electronic states of *individual* ions, the quantized states of *collective* vibrational motion of ions along the trap are also employed. These states represent quantized eigenstates and form the normal-mode progressions (somewhat similar to the vibrational states of naturally occurring molecules). In a standard setup the trapping potential is harmonic (quadratic) and the vibrational states are all equidistant, as the states of multidimensional harmonic oscillator. Frequencies of transitions between these states are usually in the few MHz region, but selective excitation or control of these states using rf fields is impossible, because all state-to-state transitions of the "ladder" have the same frequency and occur simultaneously. In a standard setup of Cirac and Zoller, the selectivity is achieved by laser excitation from different vibrational states into the excited electronic state.

In earlier publications [18,19] we explored an alternative route for direct adiabatic control of the vibrational states of ions in a trap. This approach might help to implement purely vibrational qubits and gates. The idea is to introduce anharmonicity into the trapping potential in order to alter the spectrum of the system, which should allow addressing the vibrational states of ions in trap selectively, through rf fields of appropriate frequency, amplitude, duration, and phase. In this method of control all ions remain in the ground electronic state and no individual addressing of ions is necessary. The phase of vibrational motion can also be controlled, which makes this approach suitable for quantum computation. The time-varying control fields can be designed using the optimal control theory (or the feedback loop in the experiment) in order to optimize the desired control tasks, such as state-to-state transitions, qubit flips, quantum gates, etc.

In Refs. [18] and [19] we showed that vibrational states of a single ion can be easily controlled this way if a *quartic* potential term is introduced in addition to the *quadratic* trapping potential. We carried out the computational studies and modeling of one qubit encoded into the vibrational states of a single $^{111}Cd^+$ ion in such an anharmonic trap, with $|0\rangle$ and $|1\rangle$ states of the qubit being the ground and first excited vibrational states of the system, respectively. The optimal control theory was employed in order to "shape" the control pulses for major quantum gates. Anharmonicity of the spectrum was characterized by the anharmonicity parameter, Δ, and it was found that when the value of Δ reaches $\sim$1% of the frequency ($\Omega/2\pi = 2.77$ MHz),very accurate control is possible by the simply shaped pulses. The duration of the predicted pulses was 10 μs; the field amplitudes were on the order of 0.1 V/m. It was concluded that a practical realization of such a control scenario is within the reach of today's technology.

Anharmonicity of the spectrum plays a key role in this method of control [18–24], but creating anharmonicities in the vibrational spectrum of a multiple-ion system appears to be less trivial. In the first paper of this series, Ref. [19], we considered a three-ion system in a linear trap arrangement and tried to determine what functional form of the trapping potential is needed in order to create anharmonicities sufficient for control (e.g., $\Delta \sim 1\%\Omega$). It was found that, in the three-ion case, adding quartic terms to the quadratic trapping potential does not permit us to achieve the necessary amount of vibrational anharmonicity. Even if a purely quartic (strongly anharmonic) trapping potential is used, the normal-mode progressions of vibrational states remain nearly harmonic (e.g., $\Delta \sim 0.001\%\Omega$). This surprising result was explained by deformation of the normal vibration modes in the nonharmonic multidimensional potentials [19].

*Corresponding author: Dmitri.Babikov@mu.edu

Further attempts to identify a three-ion system with a sufficiently anharmonic vibrational spectrum led us to consider a trapping potential of the following form:

$$U(z) = -\alpha z^2 + \beta z^4, \tag{1}$$

where α and β are two positive numbers. Note that the quadratic term in Eq. (1) is inverted and represents a repulsive, nontrapping contribution. By tuning the values of parameters α and β in Eq. (1), one can create a very flat strongly anharmonic trap. The shape of such a potential, the equilibrium positions of three ions, and the equilibrium energy of the system are shown in Fig. 1(a). The values of α and β are chosen such that the quadratic term creates a small repulsive "hill" in a trapping well, dominated by the quartic term. The energy of the system is well above the top of the hill. Analysis of the normal vibration modes in such a trap revealed very significant anharmonicities. The center-of-mass motion mode is the most anharmonic ($\Delta \sim 1\%\Omega$), while the symmetric stretching and the asymmetric stretching modes are less anharmonic. It was concluded that this system is a promising candidate for implementing the direct adiabatic control scenario. Note that creating the trapping potentials such as in Eq. (1) is quite feasible in the experiment [3].

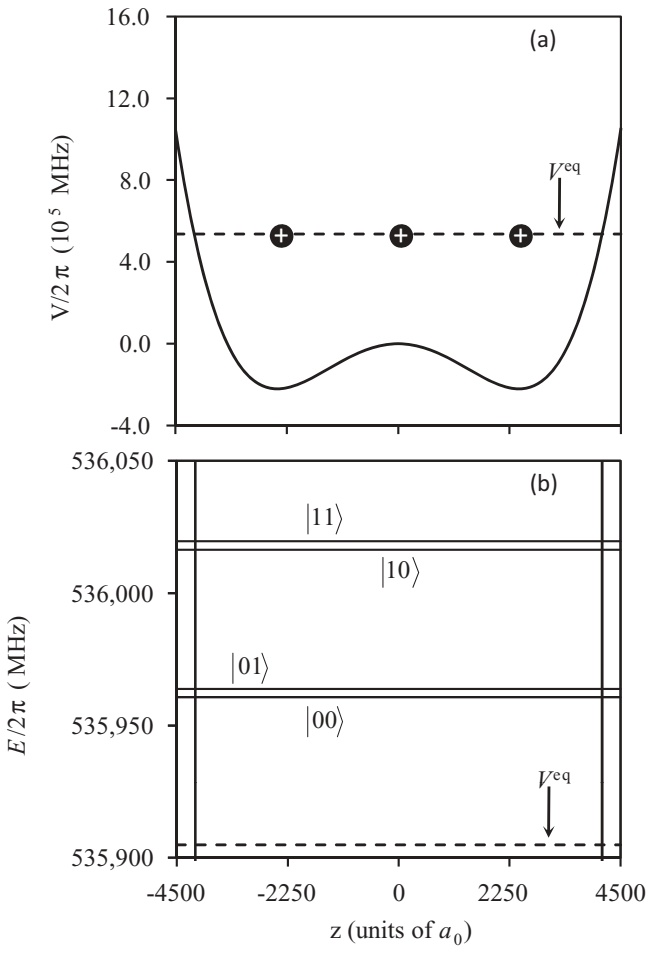

FIG. 1. (a) Equilibrium positions of ions and minimum energy of a three-ion string trapped in a flat anharmonic potential of the form $-\alpha z^2 + \beta z^4$. (b) Vibrational spectrum of this system and the encoding of two-qubit states proposed in this work.

In this paper, the second paper of the series, we study further the system of three ions in a trap of Eq. (1) [Fig. 1(a)], with a focus on controllability issues, and explore computationally the following opportunity. We propose to create a purely vibrational two-qubit system by encoding the first (control) qubit into the states of a less anharmonic asymmetric stretching vibration mode, while the second qubit is encoded into the states of a more anharmonic center-of-mass motion mode. The third mode of this system, symmetric stretching, appears to be dark and should not interfere. Using the tools of the optimal control theory, we carry out modeling of this two-qubit system and derive rf fields for direct adiabatic control of state-to-state transitions. Pulses for the major quantum gates are obtained and properties of the qubit transformations in this system are explored.

This paper is organized as follows: In Sec. II we review our theoretical framework, including the Hamiltonian of the system, the method of calculating vibrational states in an anharmonic potential, the state-to-state transition moment matrix, and the optimal control theory. Optimization of pulses for gates NOT, controlled-NOT (CNOT), and the Hadamard transform is presented in Sec. III. Major findings are summarized as conclusions in Sec. IV.

II. THEORETICAL FRAMEWORK

A. Eigenstates of the system

For a system of three ions in a linear Paul trap the vibrational Hamiltonian is [3,19]

$$H_{\text{trap}} = T + V_{\text{trap}} + V_{\text{Coulomb}} - V^{\text{eq}}. \tag{2}$$

Here the kinetic energy operator is

$$T = -\frac{1}{2m_1}\frac{\partial^2}{\partial z_1^2} - \frac{1}{2m_2}\frac{\partial^2}{\partial z_2^2} - \frac{1}{2m_3}\frac{\partial^2}{\partial z_3^2}, \tag{3}$$

the potential energy of ions in a trap is

$$V_{\text{trap}} = q_1 U(z_1) + q_2 U(z_2) + q_3 U(z_3), \tag{4}$$

the Coulomb repulsion energy is

$$V_{\text{Coulomb}} = \frac{q_1 q_2}{|z_2 - z_1|} + \frac{q_1 q_3}{|z_3 - z_1|} + \frac{q_2 q_3}{|z_3 - z_2|}, \tag{5}$$

and V^{eq} is a constant energy shift described below. A set of three Cartesian coordinates (z_1, z_2, z_3) is used to describe positions of three ions along the axis of the linear trap. The radial motion of ions in a trap is considered to be sufficiently decoupled from the axial motion and is not included in the model. This is a very reasonable approximation for a flat trap with a small number of ions. In this work we assume that all ions are equivalent and use the same masses and charges: $m_n = m = 111$ amu, the mass of the $^{111}Cd^+$ ion, and $q_n = q = +1e$, its electric charge. The trapping potential $U(z)$ of Eq. (1) is employed. The values of coefficients α and β, as suggested in the previous work, are $\alpha = 0.466\ \text{MHz}/a_0^2$ and $\beta = 3.912 \times 10^{-8}\ \text{MHz}/a_0^4$. The energy shift by $V^{\text{eq}}/2\pi = 5.359 \times 10^5$ MHz in Eq. (2) is used for convenience. Its

value represents the equilibrium (minimum) energy of the system:

$$V^{\rm eq} = V_{\rm trap}\left(z_1^{\rm eq},z_2^{\rm eq},z_3^{\rm eq}\right) + V_{\rm Coulomb}\left(z_1^{\rm eq},z_2^{\rm eq},z_3^{\rm eq}\right). \quad (6)$$

The equilibrium positions of ions $(z_1^{\rm eq},z_2^{\rm eq},z_3^{\rm eq})$ were determined numerically using the Newton-Raphson method [19]: $z_1^{\rm eq} = -2.862 \times 10^3 a_0$, $z_2^{\rm eq} \approx 0$, and $z_3^{\rm eq} = 2.862 \times 10^3 a_0$.

The time-independent Schrödinger equation for this system is solved numerically. All details can be found in Ref. [19]; only a brief summary is given here. The Hamiltonian of Eq. (2) is transformed from the Cartesian coordinates (z_1,z_2,z_3) to the normal-mode "unscaled" coordinates $(\zeta_1,\zeta_2,\zeta_3)$ by

$$\begin{pmatrix} z_1 \\ z_2 \\ z_3 \end{pmatrix} = \mathbf{A} \begin{pmatrix} (\omega_1/\omega_1)\zeta_1 \\ (\omega_1/\omega_2)\zeta_2 \\ (\omega_1/\omega_3)\zeta_3 \end{pmatrix} + \begin{pmatrix} z_1^{\rm eq} \\ z_2^{\rm eq} \\ z_3^{\rm eq} \end{pmatrix}, \quad (7)$$

using the matrix of normal-mode eigenvectors,

$$\mathbf{A} = \begin{pmatrix} a_{11} & a_{12} & a_{13} \\ a_{21} & a_{22} & a_{23} \\ a_{31} & a_{32} & a_{33} \end{pmatrix}. \quad (8)$$

and the normal-mode frequencies $(\omega_1,\omega_2,\omega_3)$, derived from the normal-mode analysis at the minimum energy point $(z_1^{\rm eq},z_2^{\rm eq},z_3^{\rm eq})$. The wave function of the system is expressed in these coordinates, $\psi_v(\zeta_1,\zeta_2,\zeta_3)$, and is expanded in terms of the three-dimensional direct-product basis set of one-dimensional harmonic oscillator functions in ζ_1, ζ_2 and ζ_3:

$$\psi_v(\zeta_1,\zeta_2,\zeta_3) = \sum_{ijk} C_{v_{ijk}} \varphi_i(\zeta_1)\varphi_j(\zeta_2)\varphi_k(\zeta_3). \quad (9)$$

An efficient basis set is constructed using frequencies $(\omega_1,\omega_2,\omega_3)$ and effective masses (μ_1,μ_2,μ_3) of the normal modes. Numerical diagonalization of the Hamiltonian matrix in this basis set gives accurate eigenvalues and eigenfunctions. These were tabulated and are available from Ref. [19]. Analysis of wave functions allowed to assign the normal-mode quantum numbers (v_1,v_2,v_3) to these states and fit the spectrum by a multidimensional Dunham formula [25]. Coefficients of the fit gave us values of frequencies of the system [19],

$$\begin{aligned} \Omega_1/2\pi &= 2.738 \text{ MHz}, \\ \Omega_2/2\pi &= 54.580 \text{ MHz}, \\ \Omega_3/2\pi &= 54.886 \text{ MHz}, \end{aligned} \quad (10)$$

and the following set of intramode anharmonicities,

$$\begin{aligned} \Delta_1/2\pi &= -4.361 \times 10^{-2} \text{ MHz}, \\ \Delta_2/2\pi &= 1.106 \times 10^{-3} \text{ MHz}, \\ \Delta_3/2\pi &= -1.371 \times 10^{-3} \text{ MHz}, \end{aligned} \quad (11)$$

for the three normal vibration modes. The intermode anharmonicities (couplings) are also important for the control; their values are

$$\begin{aligned} \Delta_{13}/2\pi &= -4.871 \times 10^{-3} \text{ MHz}, \\ \Delta_{12}/2\pi &= -1.102 \times 10^{-2} \text{ MHz}, \\ \Delta_{23}/2\pi &= 3.872 \times 10^{-2} \text{ MHz}. \end{aligned} \quad (12)$$

From these results we see that mode 1, the center-of-mass motion mode, is the most anharmonic ($\Delta_1 = 1.6\%\Omega_1$). We expect this mode to be the easiest to control and, based on this property, we choose to encode states of the main qubit (second qubit) into states of this mode. Mode 3, the asymmetric stretching mode, is considerably less harmonic ($\Delta_3 = 0.003\%\Omega_3$) and would be impossible to control by itself. However, we can try to employ this mode for encoding states of the *control* qubit (first qubit). Note that frequencies of these two modes are very different, 2.738 and 54.886 MHz, which should simplify the control. Although it may appear that the frequency of mode 2, the symmetric stretching mode, is dangerously close to the frequency of mode 3, it should not be a problem since mode 2 appears to be dark (see Sec. II D below) and should not interfere.

It is reasonable to choose two lower states (the ground and the first excited vibrational states) of each active mode to represent states $|0\rangle$ and $|1\rangle$ of the corresponding qubit. So, the following mapping between the vibrational states of the three-ion string, labeled by three normal-mode quantum numbers (v_1,v_2,v_3), and the four states of the two-qubit system is proposed:

$$\begin{aligned} |00\rangle &\Leftrightarrow (0,0,0); \quad |01\rangle \Leftrightarrow (1,0,0); \\ |10\rangle &\Leftrightarrow (0,0,1); \quad |11\rangle \Leftrightarrow (1,0,1). \end{aligned} \quad (13)$$

Energies of these states are shown in Fig. 1(b) relative to the classical minimum energy of the system $V^{\rm eq}$. Note that energy of the ground state (0,0,0) above $V^{\rm eq}$ represents the quantum zero-point energy of the system.

We would like to note that the notions of the normal modes are used here for qualitative purposes only, mostly for convenience of discussion. Their frequencies, anharmonicities, and the normal-mode quantum numbers are all approximate moieties. In reality we are dealing with exact eigenstates of the system, we use numerically accurate values of their energies and wave functions, and we encode states of the two-qubit system into these exact eigenstates.

B. Method of control

In order to control the vibrational states of ions in an anharmonic trap, we propose to apply a time-dependent electric field $\varepsilon(z,t)$ along the axis of the trap. When this control field is introduced, the full Hamiltonian of the system becomes

$$H = H_{\rm trap} + q_1\Phi(z_1,t) + q_2\Phi(z_2,t) + q_3\Phi(z_3,t), \quad (14)$$

where

$$\Phi(z_n,t) = -\int_0^z \varepsilon(z_n,t)dz \quad (15)$$

is the electric potential of the control field at the position of each ion. The easiest approach for the control is to create a spatially homogeneous field with the time-dependent amplitude $\varepsilon(t)$, which results in a linear control potential with the time-dependent slope, $\Phi(z,t) = -z\varepsilon(t)$, and leads to a simple expression for the control Hamiltonian:

$$H = H_{\rm trap} - (q_1z_1 + q_2z_2 + q_3z_3)\varepsilon(t). \quad (16)$$

For convenience, we introduce the dipole moment function of ions as

$$d(z_1,z_2,z_3) = q_1 z_1 + q_2 z_2 + q_3 z_3. \tag{17}$$

Using this definition, the control Hamiltonian of Eq. (16) can be rewritten as

$$H = H_{\text{trap}} - \varepsilon(t) d, \tag{18}$$

For the case of three equivalent ions with charge q, such as the system studied in this work, the dipole moment function is very simple:

$$d(z_1,z_2,z_3) = q(z_1 + z_2 + z_3). \tag{19}$$

C. Optimal control theory

The purpose of computational pulse optimization is to derive the time dependence (shape) of the control pulse that permits to achieve the transfer of population from a given initial, ϕ_i, to a chosen final vibrational state, ϕ_f. The time-dependent wave function of the system driven by the pulse is denoted as $\vec{\psi}(t)$ and, ideally, we want to obtain $\vec{\psi}(T) = \phi_f$ starting with $\vec{\psi}(0) = \phi_i$, where T is the duration of the pulse. In practice, the measure of success of the control pulse is the value of the overlap $|\langle\vec{\psi}(T)|\phi_f\rangle|^2$ between the actual final wave function and the wave function of the target state. The control pulse designed to induce *multiple* state-to-state transitions (e.g., different transitions of the quantum gate) can be assessed by the value of cumulative transition probability, defined as

$$P = \frac{1}{M}\sum_m \left|\langle\vec{\psi}^m(T)|\phi_f^m\rangle\right|^2. \tag{20}$$

Here the index m labels M transitions we want to optimize simultaneously, $1 \leqslant m \leqslant M$. For example, for optimization of the gate NOT we can choose $|0\rangle \to |1\rangle$ and $|1\rangle \to |0\rangle$ transitions ($M = 2$) and define $\phi_i^{(1)} = |0\rangle$, $\phi_f^{(1)} = |1\rangle$, and $\phi_i^{(2)} = |1\rangle$, $\phi_f^{(2)} = |0\rangle$, respectively. For more complicated gates we have to include more transitions into the simultaneous optimization procedure. The M transitions chosen for pulse optimization are sometimes called the *training set* [26,27].

The optimal control field $\varepsilon(t)$ is obtained by maximizing a multitarget functional defined as [28]

$$J = P - \int_0^T \alpha(t)|\varepsilon(t)|^2\,dt - \sum_m 2\text{Re}\left\{\langle\vec{\psi}^m(T)|\phi_f^m\rangle\int_0^T \langle\vec{\psi}^m(T)|iH + \frac{\partial}{\partial t}|\vec{\psi}^m(t)\rangle dt\right\}. \tag{21}$$

The second term in Eq. (21) is included in order to minimize the energy of the pulse and constrain its smooth switching on and off. The penalty function $\alpha(t) = \alpha_0/s(t)$, where α_0 is a constant penalty factor and $s(t) = \sin^2(\pi t/T)$ is a smooth envelope function, allows to reduce the field amplitude at the beginning and the end of the pulse. Minimization of the last term in Eq. (21) ensures that the evolution of the wave function obeys the time-dependent Schrödinger equation. H is the Hamiltonian of the system, Eq. (14).

Variations of the functional in Eq. (21) with respect to $\overleftarrow{\psi}^m(t)$, $\vec{\psi}^m(t)$, and $\varepsilon(t)$ lead to the following:

(i) a set of M Schrödinger equations,

$$i\frac{\partial}{\partial t}\vec{\psi}^m(t) = \hat{H}\vec{\psi}^m(t), \quad \vec{\psi}^m(0) = \phi_i^m, \tag{22}$$

to propagate M wave functions $\vec{\psi}^m(t)$ from $t = 0$ to $t = T$ independently, each with its own initial state ϕ_i^m as boundary condition;

(ii) a set of M Schrödinger equations,

$$i\frac{\partial}{\partial t}\overleftarrow{\psi}^m(t) = \hat{H}\overleftarrow{\psi}^m(t), \quad \overleftarrow{\psi}^m(T) = \phi_f^m, \tag{23}$$

to propagate M wave functions $\overleftarrow{\psi}^m(t)$ from $t = T$ to $t = 0$ (backward in time) each with its own final state ϕ_f^m as boundary condition; and

(iii) one equation for the universal field that drives all these $2M$ transitions:

$$\varepsilon(t) = -\frac{s(t)}{\alpha_0}\text{Im}\sum_m \langle\vec{\psi}(t)|\overleftarrow{\psi}(t)\rangle\langle\overleftarrow{\psi}(t)|d|\vec{\psi}(t)\rangle. \tag{24}$$

The field $\varepsilon(t)$ of Eq. (24) is improved iteratively, using information from the forward and backward propagated wave functions $\vec{\psi}^m(t)$ and $\overleftarrow{\psi}^m(t)$ of Eqs. (22) and (23). Note that $2M$ Schrödinger equations in (22) and (23) are coupled only through the field $\varepsilon(t)$ of Eq. (24).

The time propagation of the Schrödinger equation is carried out numerically by expanding the wave function over the basis set of system eigenstates (calculated numerically, see Sec. II A),

$$\psi(t) = \sum_v a_v(t)e^{-iE_v t}\psi_v, \tag{25}$$

and solving a set of coupled equations for the time-dependent coefficients $a_v(t)$ using the fourth-order Runge-Kutta method [29].

D. Transition matrix

The integral $\langle\overleftarrow{\psi}|d|\vec{\psi}\rangle$ in Eq. (24) can be expressed through time-dependent coefficients $a_v(t)$ of expansion (25) and elements of the dipole moment matrix:

$$M_{v,v'} = \langle\psi_v(\zeta_1,\zeta_2,\zeta_3)\,|d(z_1,z_2,z_3)|\,\psi_{v'}(\zeta_1,\zeta_2,\zeta_3)\rangle\,. \tag{26}$$

Note that in this formula the wave functions of eigenstates are expressed, and the integration is carried out, using the normal-mode coordinates $(\zeta_1,\zeta_2,\zeta_3)$, while the dipole moment function, as defined in Eq. (19), is expressed in Cartesian coordinates (z_1,z_2,z_3). The dipole moment function should be converted into the normal-mode coordinates using the transformation of Eq. (7):

$$\begin{aligned} d &= q(z_1 + z_2 + z_3) \\ &= q\frac{\omega_1}{\omega_1}(a_{11} + a_{21} + a_{31})\zeta_1 + q\frac{\omega_1}{\omega_2}(a_{12} + a_{22} + a_{32})\zeta_2 \\ &\quad + q\frac{\omega_1}{\omega_3}(a_{13} + a_{23} + a_{33})\zeta_3 + q\left(z_1^{\text{eq}} + z_2^{\text{eq}} + z_3^{\text{eq}}\right). \end{aligned} \tag{27}$$

Note that for the system of three equivalent ions the last term in Eq. (27) vanishes simply because $z_1^{\text{eq}} = -z_3^{\text{eq}}$ and $z_2^{\text{eq}} = 0$.

The symmetric stretching mode, mode 2, is characterized by $a_{12} = -a_{32}$ and $a_{22} = 0$, which means that the second term in Eq. (27) also vanishes. Thus, the dipole moment function does not depend on ζ_2 at all, which means that mode 2 is dark. The dependence of $d(\zeta_1,\zeta_3)$ on both ζ_1 and ζ_3 is linear:

$$d(\zeta_1,\zeta_3) = q(a_{11}+a_{21}+a_{31})\zeta_1 + q\frac{\omega_1}{\omega_3}(a_{13}+a_{23}+a_{33})\zeta_3. \tag{28}$$

Due to different frequencies and properties of the normal-mode eigenvectors, the slope of $d(\zeta_1,\zeta_3)$ for mode 1 is more than order of magnitude sharper than for mode 3.

The dipole moment function of Eq. (27) and the wave functions of Eq. (9) are substituted into Eq. (26). Using properties of the basis set functions [30], the integration in Eq. (26) is carried out analytically and elements of the dipole moment matrix are expressed through coefficients $C_{v_{ijk}}$ of the basis set expansion:

$$\begin{aligned} M_{v,v'} = {} & (a_{11}+a_{21}+a_{31})q\sum_{ijk} C^*_{v_{ijk}} \sum_{i'j'k'} C_{v'_{i'j'k'}} \frac{(\sqrt{i}\delta_{i,i'+1}+\sqrt{i+1}\delta_{i,i'-1})}{\sqrt{2\mu_1\omega_1}}\delta_{j,j'}\delta_{k,k'} \\ & + \frac{\omega_1}{\omega_2}(a_{12}+a_{22}+a_{32})q\sum_{ijk} C^*_{v_{ijk}} \sum_{i'j'k'} C_{v'_{i'j'k'}} \frac{(\sqrt{j}\delta_{j,j'+1}+\sqrt{j+1}\delta_{j,j'-1})}{\sqrt{2\mu_2\omega_2}}\delta_{i,i'}\delta_{k,k'} \\ & + \frac{\omega_1}{\omega_3}(a_{13}+a_{23}+a_{33})q\sum_{ijk} C^*_{v_{ijk}} \sum_{i'j'k'} C_{v'_{i'j'k'}} \frac{(\sqrt{k}\delta_{k,k'+1}+\sqrt{k+1}\delta_{k,k'-1})}{\sqrt{2\mu_3\omega_3}}\delta_{i,i'}\delta_{j,j'} \\ & + \left(z_1^{\mathrm{eq}}+z_2^{\mathrm{eq}}+z_3^{\mathrm{eq}}\right)q\sum_{ijk} C^*_{v_{ijk}} \sum_{i'j'k'} C_{v'_{i'j'k'}}\delta_{i,i'}\delta_{j,j'}\delta_{k,k'}. \end{aligned} \tag{29}$$

Here $(\omega_1,\omega_2,\omega_3)$ are frequencies and (μ_1,μ_2,μ_3) are effective masses of the basis set functions [19], i.e., normal modes of the trap. For the system studied in this work the second and last terms of this sum vanish exactly (due to properties of the dipole moment function; see above) and are given here only for the purpose of generality.

The usual symmetry considerations are applicable to the transition matrix of Eq. (29). The dipole moment function $d(\zeta_1,\zeta_3)$ is an asymmetric (linear) function of both ζ_1 and ζ_3. Thus, the matrix elements are nonzero only for transitions between states of different symmetries (e.g., symmetric-to-asymmetric states and vice versa), leading to the following selection rules,

$$\Delta v = \pm 1,\ \pm 3,\ \pm 5, \text{ etc.}, \tag{30}$$

for both modes 1 and 3. Since the system is only weakly anharmonic, the $\Delta v = \pm 1$ transitions are much brighter than the $\Delta v = \pm 3,\ \pm 5$, etc. transitions.

Note that the symmetric stretching mode is dark only in the case when a spatially homogeneous field is used, as assumed in this work. Creating a quadrupole potential would allow controlling the symmetric stretching mode, too. This opportunity will be studied theoretically and computationally in a future work.

III. RESULTS AND DISCUSSION

It is understood that it may be difficult to create in the experiment the time-varying field $\varepsilon(t)$ exactly as recommended by theory, and that the experimental implementation may have some practical constraints not included into our model. Still, it is desirable to have a theoretical benchmark of the approach, before any practical implementation is attempted, in order to see how difficult or easy would it be to implement this method of control.

A. Gate NOT on second qubit

For this gate the training set of four transitions was chosen as

$$\mathrm{NOT}\,|00\rangle \rightarrow |01\rangle\,, \tag{31}$$

$$\mathrm{NOT}\,|01\rangle \rightarrow |00\rangle\,, \tag{32}$$

$$\mathrm{NOT}\,|10\rangle \rightarrow |11\rangle\,, \tag{33}$$

$$\mathrm{NOT}\,|11\rangle \rightarrow |10\rangle\,. \tag{34}$$

Recall that in our approach the qubits are encoded into *collective* vibration modes, not into individual ions, and the control field is applied to the entire system, not to the individual qubits. For this reason, the state of the first qubit should be reflected also in the training set of transitions, even if we are trying to optimize the pulse for controlling just the second qubit. In this sense our gates are global. The first two transitions of the training set describe the action of the gate NOT on the second qubit, with the first qubit being in state $|0\rangle$, while next two transitions of the training set describe the gate NOT on the second qubit with the first qubit being in state $|1\rangle$. Due to anharmonicities, the frequencies of the corresponding $|00\rangle \leftrightarrow |01\rangle$ and $|10\rangle \leftrightarrow |11\rangle$ transitions are slightly different.

The optimization procedure is not fully automated. The pulse duration and the maximum allowed field amplitude should be tuned manually. A number of independent computational experiments were carried out with different values of the target time in the range between 2 and 20 μs and different values of the penalty factor between 10^{11} and 10^{13}. The following values led to the simplest pulse shape and were finally adopted for the gate NOT: $T = 4$ μs and $\alpha = 2.0 \times 10^{12}$. A very large number of iterations, 4000 forward-backward

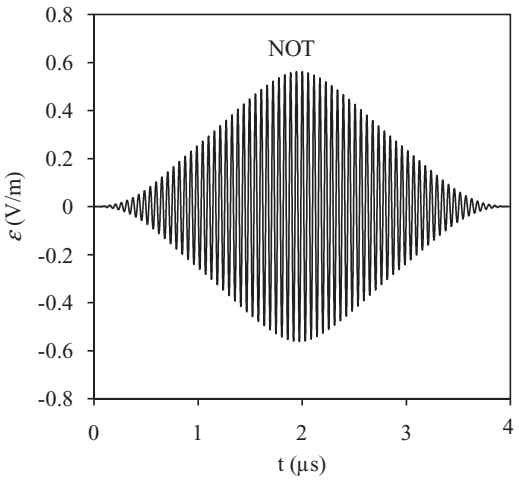

FIG. 2. Optimally shaped pulse for the gate NOT.

loops, were needed in order to converge the pulse shape. The length of the time step in the wave-packet propagation was on the order of 0.5 ns (9000 time steps in total).

The 4-μs pulse derived for the gate NOT on the second qubit is presented in Fig. 2. The pulse is quite symmetric and its shape is simple, and the maximum field is achieved in the middle of the pulse. This shape reflects the envelope function (see Sec. II C) used to switch the pulse on and off smoothly. The amplitude of the electric field does not exceed 0.57 V/m. Such pulses should be relatively easy to produce in the experiment.

Figure 3 shows the evolution of state populations during the pulse. The four frames of the picture correspond to the four transitions of the training set. We see that, overall, the population transfer is quite direct, in the sense that the population of the initial state(s) is monotonically transferred to the final state(s), without any reverse transfer. Note, however, that the system does not behave as an isolated four-state system of two qubits. The upper states of the normal-mode progressions can gain some population during the pulse. Here, the states $|02\rangle$ and $|12\rangle$ are excited most significantly (populations exceeds 0.1), which can be seen in Fig. 3 without any magnification. However, the system is well controlled—by the end of the pulse all of the population is dumped into the target state(s) of two qubits. The value of cumulative transition probability, as defined in Eq. (20), reaches $P = 0.996$.

A Fourier analysis of the pulse in Fig. 2 shows that its spectrum is dominated by structure in the $\Omega/2\pi = 2.7$–3.2 MHz region, which corresponds to excitation of one quantum of vibration in the second qubit. The structure is asymmetric. Its most intensive peak corresponds to a frequency of the $|0\rangle \leftrightarrow |1\rangle$ transition. A wing, composed of series of less intense peaks, extends into the blue part of spectrum and covers the $|1\rangle \leftrightarrow |2\rangle$, $|3\rangle \leftrightarrow |4\rangle$, and $|4\rangle \leftrightarrow |5\rangle$ transitions, which means that this pulse is trying to control *selectively* the ladder of the transitions (an anharmonic oscillator). Note that all these transitions are well resolved by the pulse—the widths of peaks in the spectrum are narrower than the frequency differences. However, the transitions $|00\rangle \leftrightarrow |01\rangle$ and $|10\rangle \leftrightarrow |11\rangle$, etc., are not resolved. Frequencies of these transitions are very close to each other because the anharmonicity of the first qubit is very small. The widths of peaks in the spectrum are

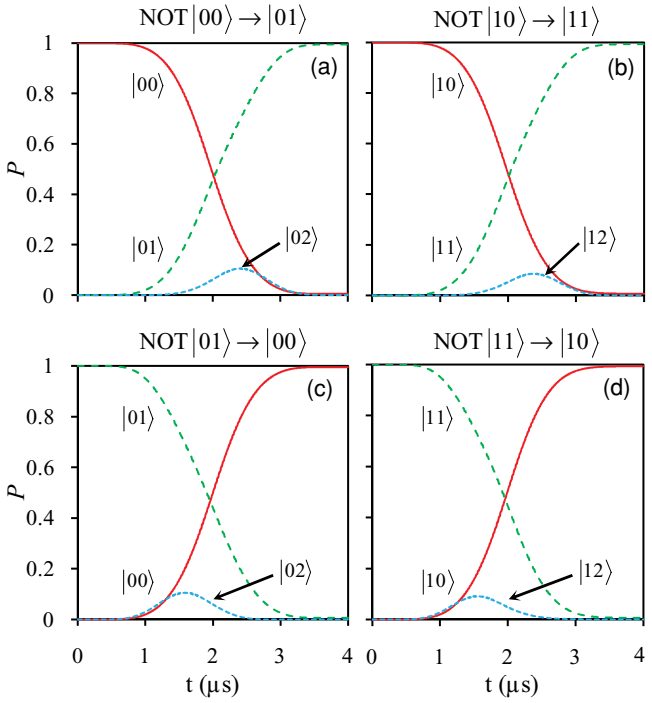

FIG. 3. (Color online) Evolution of state populations during the gate NOT. The four frames of this figure correspond to the four transitions optimized as a training set.

much broader than this frequency difference, which means that the $|00\rangle \leftrightarrow |01\rangle$ and $|10\rangle \leftrightarrow |11\rangle$ transitions are controlled *together*, rather than selectively.

The intensity of the signal near the frequency of the $|2\rangle \leftrightarrow |3\rangle$ transition is suppresed relative to others, which explains why the population of state $|3\rangle$ remains low during the pulse. A Fourier analysis shows no frequency components near 2Ω for the second qubit, consistent with the selection rules of Eq. (30), and shows only a small intensity near the $3\Omega/2\pi = 8.8$ MHz region, the $|0\rangle \leftrightarrow |3\rangle$ transition in the second qubit, which is consistent with low population of state $|3\rangle$. Nothing in the spectrum corresponds to transitions between the states of the first qubit.

Results obtained with longer pulses indicate that an increase of the pulse duration leads to a decrease of the field amplitude and, as a consequence, to a decrease of the population of the interfering upper states. For example, we found that during a pulse optimized with $T = 20$ μs the field does not exceed 0.25 V/m, and the populations of states $|02\rangle$ and $|12\rangle$ do not exceed 0.02, while the cumulative transition probability reaches $P = 0.9998$.

B. Conditional NOT (CNOT) on second qubit

For the gate CNOT the training set of transitions is

$$\text{CNOT}\,|00\rangle \rightarrow |00\rangle\,, \tag{35}$$

$$\text{CNOT}\,|01\rangle \rightarrow |01\rangle\,, \tag{36}$$

$$\text{CNOT}\,|10\rangle \rightarrow |11\rangle\,, \tag{37}$$

$$\text{CNOT}\,|11\rangle \rightarrow |10\rangle\,. \tag{38}$$

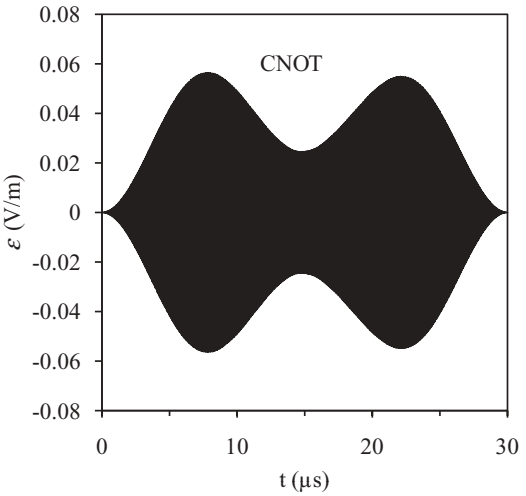

FIG. 4. Optimally shaped pulse for the gate CNOT. Low-field regime.

Experimentation with the pulse duration showed that the CNOT gate requires much longer pulses than the NOT gate. In order to obtain an accurate CNOT gate, we had to increase the pulse duration to $T = 30$ μs. The number of time steps for wave-packet propagation was increased to 18 000. Variation of the penalty factor revealed an interesting feature. It is demonstrated below using the results for two pulses, one with $\alpha = 6.0 \times 10^{12}$ and the other with $\alpha = 8.0 \times 10^{11}$.

The pulse optimized with a larger penalty factor, $\alpha = 6.0 \times 10^{12}$, is shown in Fig. 4. This pulse is simply shaped, symmetric, and consists of two time-delayed subpulses. A maximum field amplitude of ~0.06 V/m is achieved at approximately $t = 7.5$ and 22.5 μs. The state-to-state transitions driven by this pulse are shown in Fig. 5. The four frames correspond to the four transitions of the training set. When the control qubit is in state $|1\rangle$ the population transfer is monotonic and is very much direct; see Figs. 5(b) and 5(d). Only two states of the system are involved and those are states $|10\rangle$ and $|11\rangle$ of the qubit. Transitions to any upper states of the system are suppressed. When the control qubit is in state $|0\rangle$ the population transfer is not monotonic: The first subpulse creates a superposition state of $|00\rangle$ and $|01\rangle$, while the second subpulse returns the population back to the initial state(s), as required by this gate; see Figs. 5(a) and 5(c). The Cumulative accuracy of the qubit transformation is very high, P~0.9995. A Fourier analysis of the optimized pulse shows that only the $|00\rangle \leftrightarrow |01\rangle$ and $|10\rangle \leftrightarrow |11\rangle$ transitions are induced (again, together rather than selectively), while the frequencies of all other transitions are completely suppressed. Even the frequency of the $|1\rangle \leftrightarrow |2\rangle$ transition in the second qubit is entirely suppressed, which explains why the population is restricted to only states $|0\rangle$ and $|1\rangle$ of the qubit.

The fact that the transitions to the upper states of the system can be suppressed and the population is restricted to only four states of the 2×2 qubit space is very interesting. We believe that such a high selectivity is made possible by the relatively low amplitude of the field of the pulse in Fig. 4, leading to very delicate control of the vibrational excitations.

In order to support this hypothesis we present results for another pulse, optimized with a lower penalty factor

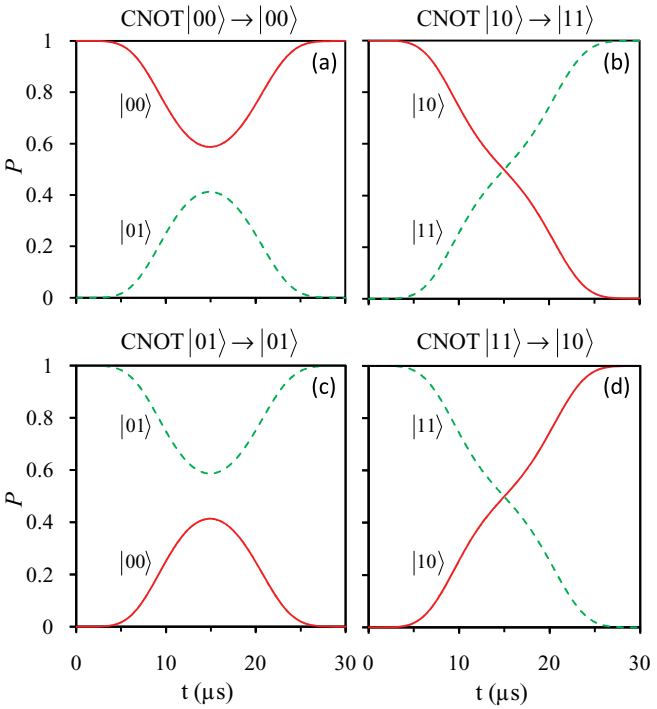

FIG. 5. (Color online) Evolution of state populations during the gate CNOT. Low-field regime. The four frames of this figure correspond to the four transitions optimized as a training set.

$\alpha = 8.0 \times 10^{11}$. In general, lowering the penalty factor allows raising amplitude of the field during the optimization procedure. The optimized pulse shape for this case is presented in Fig. 6. The maximum field amplitude of this pulse is ~0.51 V/m, approximately an order of magnitude higher as compared to the previous case. The pulse shape is much more complicated, asymmetric, and containing multiple subpulses of different amplitudes. This shape reflects the complicated evolution of state populations presented in Fig. 7. During the pulse, the populations are exchanged back and forth between the initial and the final states of the qubit, and are also transferred to the excited states of the system, $|02\rangle$ and $|12\rangle$.

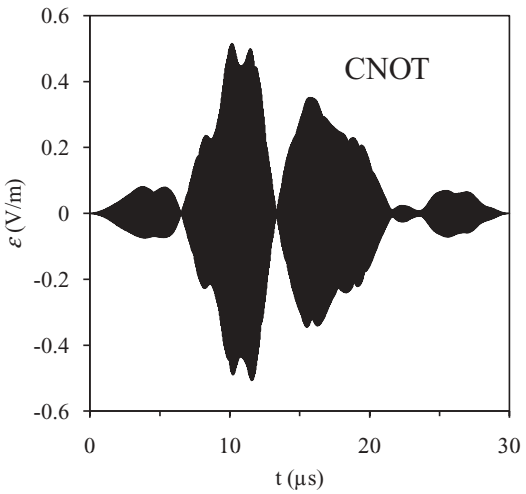

FIG. 6. Optimally shaped pulse for the gate CNOT. High-field regime.

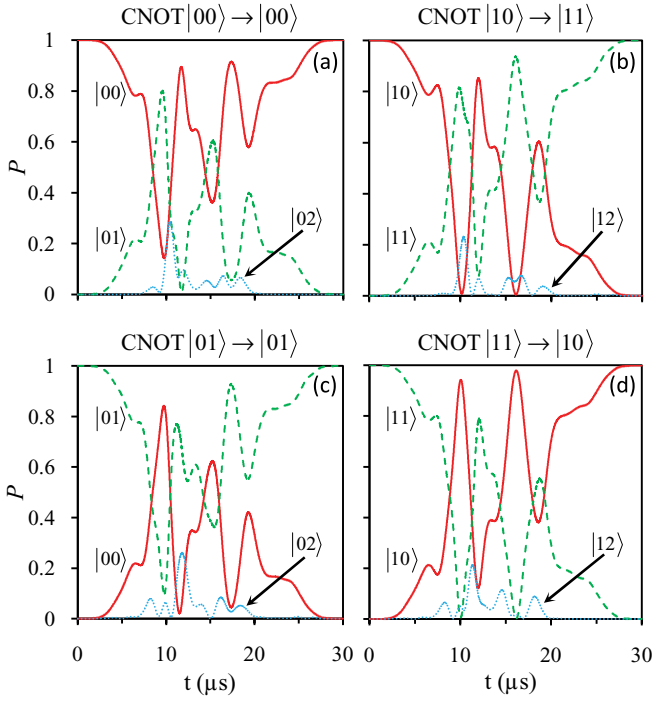

FIG. 7. (Color online) Evolution of state populations during the gate CNOT. High-field regime. The four frames of this figure correspond to the four transitions optimized as a training set.

Despite a complicated evolution during the pulse, at time $t = T$ the population is directed toward the target states, leading to a high accuracy of the qubit transformation, $P{\sim}0.9996$. A Fourier analysis of this optimized pulse shows a spectral structure that covers $|0\rangle \leftrightarrow |1\rangle$, $|1\rangle \leftrightarrow |2\rangle$ and $|3\rangle \leftrightarrow |4\rangle$, transitions in the second qubit, which clearly corresponds to control of the ladder. The frequency of the $|2\rangle \leftrightarrow |3\rangle$ transition is, again, somewhat suppressed.

Two examples of the CNOT gate presented here suggest that a careful choice of constraints on the control field, such as pulse duration and field amplitude, may be necessary in order to obtain control pulses of desirable accuracy and simplicity.

C. Hadamard transform of second qubit

The training set of transitions for the Hadamard transform of the second qubit is

$$\text{HAD}\,|00\rangle \to \frac{1}{\sqrt{2}}(|00\rangle + |01\rangle), \tag{39}$$

$$\text{HAD}\,|01\rangle \to \frac{1}{\sqrt{2}}(|00\rangle - |01\rangle), \tag{40}$$

$$\text{HAD}\,|10\rangle \to \frac{1}{\sqrt{2}}(|10\rangle + |11\rangle), \tag{41}$$

$$\text{HAD}\,|11\rangle \to \frac{1}{\sqrt{2}}(|10\rangle - |11\rangle), \tag{42}$$

$$\text{HAD}\,\frac{1}{2}(|00\rangle + |01\rangle + |10\rangle + |11\rangle) \to \frac{1}{\sqrt{2}}(|00\rangle + |10\rangle). \tag{43}$$

The fifth transition here is the sum of the first four transitions, and it is included in order to achieve control over the phases, which is essential for this gate. Note that the cumulative probability of Eq. (20) neglects the phases of transitions, since moduli squared of overlaps are used. However, the accuracy of gates such as Hadamard should be measured by a phase-sensitive moiety, such as fidelity, defined as [31,32]

$$F = \frac{1}{M^2}\left|\sum_m \langle\vec{\psi}^m(T)|\phi_f^m\rangle\right|^2. \tag{44}$$

One solution is to replace P by F in the functional of Eq. (21) and rederive the equations [31,32], but this approach was not followed here. A simpler fix to the standard procedure is to include, in addition to the four transitions of the training set, one more transition that represents the sum of the previous four transitions [21,33]. In order to ensure that the phase is indeed controlled, the fidelity of Eq. (44), rather than the probability of Eq. (20), should be monitored as a convergence criterion.

Different values of pulse duration and penalty factor were tried and the following parameters were finally adopted: $\alpha = 1.0 \times 10^{12}$ and $T = 35$ μs. The number of time steps was also adjusted to 55 000.

The optimized pulse is presented in Fig. 8. The pulse is asymmetric and consists of three subpulses of slightly different amplitudes. The maximum amplitude of the field is ~0.13 V/m. The roles of these subpulses are revealed by analysis of the state populations presented in Fig. 9. The first subpulse achieves a significant transfer of populations, creating a superposition state with probabilities close to the needed 50/50, while the second subpulse manipulates the phases of the optimized transitions (with only a minor population transfer). The third subpulse finalizes the entire transformation by a minor transfer of the remaining populations and a fine phase correction. An analysis of the phase angle of the optimized transitions supports this conclusion: During the first subpulse, phases are not controlled at all. The second subpulse reduces the phase differences monotonically to only ~30°–50°. The third subpulse reduces the phase differences to less than 4° at the end of the pulse. The cumulative transition probability of this Hadamard gate is $P{\sim}0.998$. Its fidelity is slightly lower, $F \sim 0.990$, due to a small residual difference of phases.

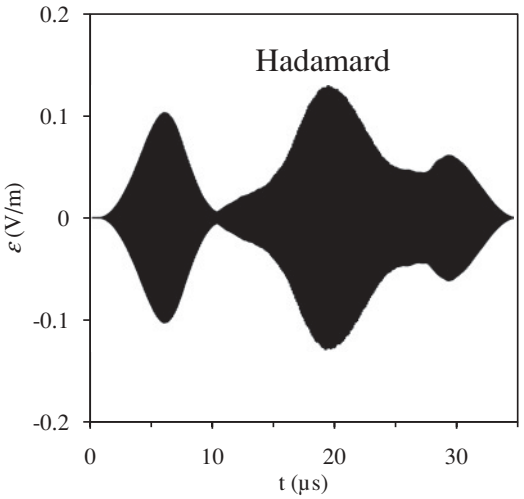

FIG. 8. Optimally shaped pulse for the Hadamard transform.

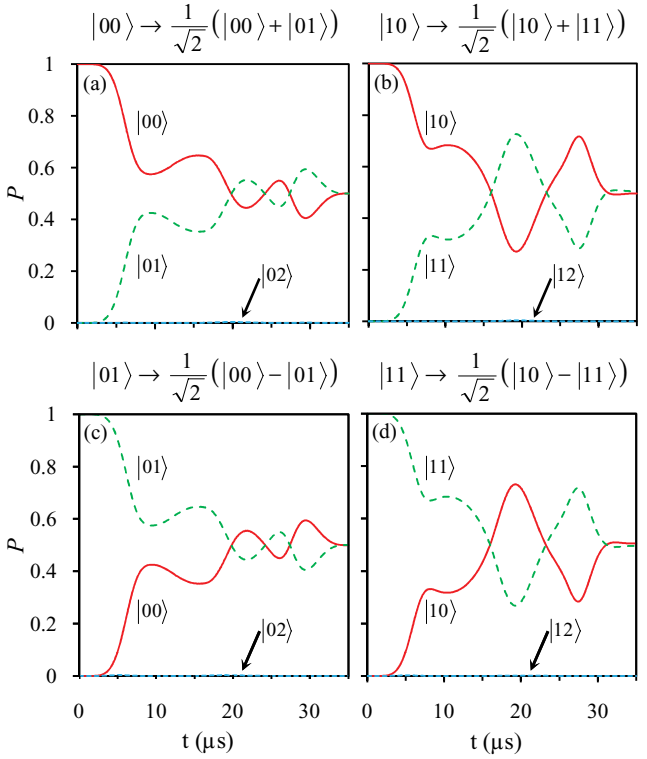

FIG. 9. (Color online) Evolution of state populations during the Hadamard transform. The four frames of this figure correspond to the four transitions optimized as a training set.

A Fourier analysis of the optimized pulse shows two spectral structures. The first structure is in the $\Omega/2\pi = 2.7$–3.0 MHz region (excitation of one quantum in the second qubit). Here the $|0\rangle \leftrightarrow |1\rangle$ transition is clearly dominant, while the $|1\rangle \leftrightarrow |2\rangle$ transition is significantly suppressed, consistent with a low population of states $|02\rangle$ and $|12\rangle$ in Fig. 9. The second spectral structure is in the $\Omega/2\pi = 54.8$–54.9 MHz region, which corresponds to excitation of one quantum of the first qubit. Transitions between the $|0\rangle \leftrightarrow |1\rangle$, $|1\rangle \leftrightarrow |2\rangle$, $|3\rangle \leftrightarrow |4\rangle$, and $|4\rangle \leftrightarrow |5\rangle$ states of the first qubit are covered by the blue-side wing of this spectral structure. We tend to state that these transitions are *partially* resolved because they all have different intensities, due to the slope of the wing and some minor oscillations of intensity.

Note that the frequency components that control the first qubit have not been observed in the optimized NOT and CNOT pulses discussed above. We found that these frequencies appear only when we include the fifth transition into the training set [e.g., Eq. (43)] in order to control phases of the optimized transitions. The pulses optimized for such truly coherent manipulations of the qubit states always contain frequency components for control of both qubits of the two-qubit system.

IV. CONCLUSIONS

In this paper we carried out an optimal control study of a system of multiple ions in an anharmonic linear trap. The method of encoding qubits into the quantized collective motional states of the linear ion string was proposed and explored computationally. The time-varying rf fields were used to achieve adiabatic control over these states.

Although all ions are identical, the vibration modes of the ion string are different and the qubits, encoded into these modes, are also different. A numerical analysis of frequencies and anharmonicities of the vibration modes was used to identify the modes most suitable for encoding qubits. It was shown that in a strongly anharmonic trap, obtained by combining a repulsive quadratic with attractive quartic potentials, the center-of-mass motion mode is the most anharmonic. It is most suitable for encoding states of the main qubit. The control qubit can be encoded into a less anharmonic asymmetric stretching mode. The symmetric stretching mode remains dark in our approach.

The optimal control theory was used to derive pulses for a set of universal quantum gates. It was shown that if the parameters of the pulse, such as pulse duration and maximum field amplitude, are carefully chosen, the qubit transformations (gates) are accurate and the pulses are simple. The durations of the pulses obtained were in the 4–40 μs range. Amplitudes of the control fields were on the order of 0.1 V/m.

Only one set of parameters for the shape of the trap was considered in this paper. It seems feasible, however, to further increase the anharmonicity of the vibrational spectrum of the system by changing the parameters of the trapping potential. Higher anharmonicities, in turn, should simplify control and allow the derivation of more accurate and shorter gate pulses. Exploring a system of more than three ions offers more opportunities. There should be more than one anharmonic mode that can be efficiently controlled and used for encoding qubits. These opportunities will be explored in a future work.

ACKNOWLEDGMENTS

This work was supported by the National Science Foundation, Grant No. CHE-1012075. This research used resources of the National Energy Research Scientific Computing Center, which is supported by the Office of Science of the US Department of Energy under Contract No. DE-AC02-05CH11231. Professor Martine Gruebele at the University of Illinois at Urbana-Champaign is acknowledged for fruitful discussions.

[1] J. I. Cirac and P. Zoller, Phys. Rev. Lett. **74**, 4091 (1995).
[2] C. Monroe, D. M. Meekhof, B. E. King, W. M. Itano, and D. J. Wineland, Phys. Rev. Lett. **75**, 4714 (1995).
[3] G. D. Lin, S. L. Zhu, R. Islam, K. Kim, M. S. Chang, S. Korenblit, C. Monroe, and L. M. Duan, Europhys. Lett. **86**, 60004 (2009).
[4] D. M. Meekhof, C. Monroe, B. E. King, W. M. Itano, and D. J. Wineland, Phys. Rev. Lett. **76**, 1796 (1996).
[5] C. A. Sackett *et al.*, Nature (London) **404**, 256 (2000).
[6] J. J. Garcia-Ripoll, P. Zoller, and J. I. Cirac, Phys. Rev. Lett. **91**, 157901 (2003).
[7] F. Schmidt-Kaler, H. Haeffner, R. Riebe, S. Gulde, G. P. T. Lancaster, T. Deuschle, C. Becher, C. F. Roos, J. Eschner, and R. Blatt, Nature (London) **422**, 408 (2003).
[8] H. Haeffner *et al.*, Nature (London) **438**, 643 (2005).

[9] D. Leibfried *et al.*, Nature (London) **438**, 639 (2005).
[10] F. Schmidt-Kaler *et al.*, Appl. Phys. B **77**, 789 (2003).
[11] P. Bushev, D. Rotter, A. Wilson, F. Dubin, C. Becher, J. Eschner, R. Blatt, V. Steixner, P. Rabl, and P. Zoller, Phys. Rev. Lett. **96**, 043003 (2006).
[12] C. Monroe and D. Wineland, Scientific American (August, 2008), p. 64.
[13] D. Leibfried, R. Blatt, C. Monroe, and D. Wineland, Rev. Mod. Phys. **75**, 281 (2003).
[14] R. Blatt and D. J. Wineland, Nature (London) **453**, 1008 (2008).
[15] K. Kim, M. S. Chang, R. Islam, S. Korenblit, L. M. Duan, and C. Monroe, Phys. Rev. Lett. **103**, 120502 (2009).
[16] K. Kim, M. S. Chang, S. Korenblit, R. Islam, E. E. Edwards, J. K. Freericks, G. D. Lin, L. M. Duan, and C. Monroe, Nature (London) **465**, 590 (2010).
[17] L. M. Duan and C. Monroe, Rev. Mod. Phys. **82**, 1209 (2010).
[18] M. Zhao and D. Babikov, Phys. Rev. A **77**, 012338 (2008).
[19] L. Wang and D. Babikov, Phys. Rev. A **83**, 022305 (2011).
[20] D. Babikov, J. Chem. Phys. **121**, 7577 (2004).
[21] M. Zhao and D. Babikov, J. Chem. Phys. **125**, 024105 (2006).
[22] M. Zhao and D. Babikov, J. Chem. Phys. **126**, 204102 (2007).
[23] Y. Y. Gu and D. Babikov, J. Chem. Phys. **131**, 034306 (2009).
[24] C. Gollub, U. Troppmann, and R. de Vivie-Riedle, New J. Phys. **8**, 48 (2006).
[25] W. Demtröder, *Molecular Physics: Theoretical Principles and Experimental Methods* (WILEY-VCH, Weinheim, 2005).
[26] D. Weidinger and M. Gruebele, Mol. Phys. **105**, 1999 (2007).
[27] D. Weidinger and M. Gruebele, Chem. Phys. **350**, 139 (2008).
[28] W. Zhu, J. Botina, and H. Rabitz, J. Chem. Phys. **108** 1953 (1998).
[29] W. H. Press, B. P. Flannery, S. A. Teukolsky, and W. T. Vetterling, *Numerical recipes: The art of scientific computing* (Cambridge University Press, New York, 1989), p. 759.
[30] B. H. Bransden and C. J. Joachain, *Introduction to Quantum Mechanics* (Longman, New York, 1989).
[31] J. P. Palao and R. Kosloff, Phys. Rev. Lett. **89**, 188301 (2002).
[32] J. P. Palao and R. Kosloff, Phys. Rev. A **68**, 062308 (2003).
[33] C. M. Tesch and R. de Vivie-Riedle, J. Chem. Phys. **121**, 12158 (2004).